*Anal. Chem.* **2006,** *78,* 7689−7696

# Estimation of the (*n,m*) Concentration Distribution of Single-Walled Carbon Nanotubes from Photoabsorption Spectra

**Nitish Nair, Monica L. Usrey, Woo-Jae Kim, Richard D. Braatz, and Michael S. Strano***

*Department of Chemical and Biomolecular Engineering, University of Illinois at Urbana−Champaign, Urbana, Illinois 61801*

**Deconvolution of the absorption spectrum of single-walled carbon nanotubes (SWNTs) into distinct (*n,m*) contributions is complicated because transition energies are closely spaced. The algorithm presented in this work attempts to simplify the problem by grouping nanotubes with similar transition energies and assigning weights to their spectral contributions. Voigt line shapes were used to fit absorption spectra of sodium dodecyl sulfate suspended HiPco SWNT and CoMoCat SWNT. Line widths for the metallic (93.42 meV) and two semiconducting regions (57.96 and 29.86 meV) were obtained from the absorption spectra of DNA-wrapped SWNT fractionated by ion-exchange chromatography. The method is used to describe the reaction kinetics of certain HiPco SWNTs upon reaction with 4-chlorobenzene diazonium and 4-hydroxybenzene diazonium salts. The code for deconvolution has been provided as open source in the Supporting Information for future modifications.**

Single-walled carbon nanotubes (SWNTs) are produced by several different methods: laser vaporization,[1] arc discharge,[2] high-pressure CO decomposition (HiPco),[3] and chemical vapor deposition.[4] Raman spectroscopy,[5,6] photoabsorption,[7,8] and spectrofluorometry[9,10] have been used to estimate the nanotube composition of samples. Early optical absorption studies on bundled nanotubes prepared by laser vaporization and the electric arc method show three broad SWNT-related peaks at approximately 0.75, 1.3, and 1.8 eV.[7,8,11] They were assigned as the first ($E_{11}^{S}$) and second ($E_{22}^{S}$) interband transitions of semiconducting nanotubes and the first transition for metallic nanotubes ($E_{11}^{M}$), respectively. Aggregation of the nanotubes, due to strongly attractive van der Waals forces, destroys fine structure in the spectra.[12] Highly resolved absorption and photoluminescence spectra were obtained after SWNTs were individually suspended in solution by surfactant adsorption.[9] These samples enabled the discovery of band gap fluorescence[9] and the spectral assignment of metallic and semiconducting species.[10,13,14] The assignment was further refined when only one of the metallic branches of the transitions was observed optically.[15]

Spectrofluorometry has been used to estimate the relative concentrations of semiconducting nanotubes in a sample.[10,16] Since metallic nanotubes and bundles of nanotubes do not fluoresce, it is not possible to detect them using this method. The absorption spectrum typically has a distinct, yet convoluted, metallic region. Additionally, in past work, we have shown that spectrofluorometric data should be interpreted with caution due to the effects of sonication-induced changes[17,18] and nanotube lengths[17] on the quantum yields. The results could also be skewed by the fact that spectrofluorometry cannot detect quenched, damaged, or defective nanotubes, which do not fluoresce at all.[19]

Previous work focused on using tight-binding theory,[20] density functional theory,[20] and excitonic calculations with the Bethe−Salpeter equation[21] for determining the absorption spectra of individual nanotubes. The absorption spectrum of SWNT bundles

* To whom correspondence should be addressed. E-mail: strano@uiuc.edu.

(1) Guo, T.; Nikolaev, P.; Thess, A.; Colbert, D. T.; Smalley, R. E. *Chem. Phys. Lett.* **1995**, *243*, 49.
(2) Journet, C.; Maser, W. K.; Bernier, P.; Loiseau, A. *Nature* **1997**, *388*, 756.
(3) Nikolaev, P.; Bronikowski, M. J.; Bradley, R. K.; Rohmund, F.; Colbert, D. T.; Smith, K. A.; Smalley, R. E. *Chem. Phys. Lett.* **1999**, *313*, 91.
(4) Cassell, A.; Raymakers, J.; Kong, J.; Dai, H. *J. Phys. Chem. B.* **1999**, *103*, 6484.
(5) Jorio, A.; Santos, A. P.; Ribeiro, H. B.; Fantini, C.; Souza, M.; Vieira, J. P. M.; Furtado, A.; Jiang, J.; Saito, R.; Balzano, L.; Resasco, D. E.; Pimenta, M. A. *Phys. Rev. B* **2005**, *72*, 075207.
(6) Jorio, A.; Fantini, C.; Pimenta, M. A.; Heller, D. A.; Strano, M. S.; Dresselhaus, M. S.; Oyama, Y.; Jiang, J.; Saito, R. *Appl. Phys. Lett.* **2006**, *88*, 023109.
(7) Jost, O.; Gorbunov, A. A.; Pompe, W.; Pichler, T.; Friedlein, R.; Knupfer, M.; Reibold, M.; Bauer, H. D.; Dunsch, L.; Golden, M. S.; Fink, J. *Appl. Phys. Lett.* **1999**, *75*, 2217−2219.
(8) Liu, X.; Pichler, T.; Knupfer, M.; Golden, M. S.; Fink, J.; Kataura, H.; Achiba, Y. *Phys. Rev. B* **2002**, 66.
(9) O'Connell, M. J.; Bachilo, S. M.; Huffman, C. B.; Moore, V. C.; Strano, M. S.; Haroz, E. H.; Rialon, K. L.; Boul, P. J.; Noon, W. H.; Kittrell, C.; Ma, J. P.; Hauge, R. H.; Weisman, R. B.; Smalley, R. E. *Science* **2002**, *297*, 593−596.
(10) Bachilo, S. M.; Strano, M. S.; Kittrell, C.; Hauge, R. H.; Smalley, R. E.; Weisman, R. B. *Science* **2002**, *298*, 2361−2366.
(11) Kataura, H.; Kumazawa, Y.; Maniwa, Y.; Umezu, I.; Suzuki, S.; Ohtsuka, Y.; Achiba, Y. *Synth. Met.* **1999**, *103*, 2555−2558.
(12) Heller, D. A.; Barone, P. W.; Swanson, J. P.; Mayrhofer, R. M.; Strano, M. S. *J. Phys. Chem. B* **2004**, *108*, 6905−6909.
(13) Strano, M. S.; Doorn, S. K.; Haroz, E. H.; Kittrell, C.; Hauge, R. H.; Smalley, R. E. *Nano Lett.* **2003**, *3*, 1091−1096.
(14) Weisman, R. B.; Bachilo, S. M. *Nano Lett.* **2003**, *3*, 1235−1238.
(15) Fantini, C.; Jorio, A.; Souza, M.; Strano, M. S.; Dresselhaus, M. S.; Pimenta, M. A. *Phys. Rev. Lett.* **2004**, 93.
(16) Bachilo, S. M.; Balzano, L.; Herrera, J. E.; Pompeo, F.; Resasco, D. E.; Weisman, R. B. *J. Am. Chem. Soc.* **2003**, *125*, 11186−11187.
(17) Heller, D. A.; Mayrhofer, R. M.; Baik, S.; Grinkova, Y. V.; Usrey, M. L.; Strano, M. S. *J. Am. Chem. Soc.* **2004**, *126*, 14567−14573.
(18) Heller, D. A.; Barone, P. W.; Strano, M. S. *Carbon* **2004**, *43*, 651−653.
(19) Usrey, M. L.; Lippmann, E. S.; Strano, M. S. *J. Am. Chem. Soc.* **2005**, *127*, 16129−16135.
(20) Zhao, Y.; Wang, X. J.; Ma, C. C.; Chen, G. H. *Chem. Phys. Lett.* **2004**, *387*, 149−154.
(21) Perebeinos, V.; Tersoff, J.; Avouris, P. *Phys. Rev. Lett.* **2004**, 92.

10.1021/ac0610917 CCC: $33.50 
Published on Web 10/13/2006

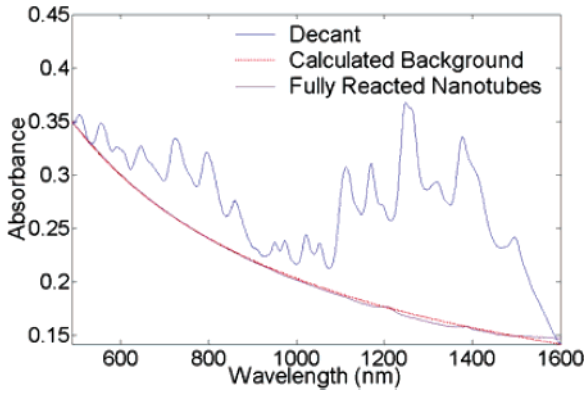


**Figure 1.** Comparison of the calculated background for the absorption spectrum of the given decant with the spectrum of completely functionalized nanotubes.

has been modeled by using the joint density of states (JDOS) of nanotubes as the starting point.[22] The more complex case of fitting the absorption spectrum of sodium dodecyl sulfate (SDS)-suspended nanotubes has been performed by two methods: (1) expressing the absorption coefficient of each nanotube as a function of its JDOS, after broadening the singularities in the JDOS profile with Gaussians;[23] (2) using Voigt profiles to approximate the spectral contribution of each nanotube, although this method was restricted to the $E_{11}^{S}$ region of the spectrum.[24]

This paper describes an algorithm that performs the deconvolution for the entire SWNT absorption spectrum using Voigt line shapes and known peak locations from the spectral assignment of metallic and semiconducting nanotubes. It yields approximate contributions of each $(n,m)$ species along with confidence intervals for each parameter, which have never been reported in any previous fitting procedure. For the first time, we have used deconvolution to extract the selective decay kinetics of representative HiPco nanotubes upon reaction with 4-chlorobenzene and 4-hydroxybenzene diazonium salts. We note that the deconvolution tool is a starting attempt at better understanding the quantitative nature of the absorption spectrum of carbon nanotubes. To refine the method, we have provided the code as open source in the Supporting Information so that future theoretical modifications can be incorporated easily.

## EXPERIMENTAL SECTION

HiPco nanotubes (Rice University, reactor run 107) were suspended in 1 wt % SDS (Sigma Aldrich) in deuterated water ($D_2O$, Sigma Aldrich) according to a previously published protocol.[9] A deuterated aqueous solution was used to eliminate water absorption features above 1400 nm in the UV−vis−NIR photoabsorption spectra. The preparation of DNA-wrapped SWNTs has been specified in past work.[25−27]

Reactions with HiPco nanotubes were conducted in 1-mL capped, unstirred, temperature-controlled quartz cuvettes (Starna) in a UV−vis−NIR spectrophotometer (Shimadzu UV-3101PC). Transient absorption spectra were generated (190−1900 nm, 1-nm step size) every 5 min, which was the integration time. The cuvette was heated using a circulating hot water bath at 45 °C. Seven additions (0.0404 mM each) of 4-hydroxybenzene diazonium (Rice University) were made at 0, 111, 292, 538, 1274, 1584, and 1885 min, respectively. Following each addition, the reaction volume was mixed thoroughly with a Pasteur pipet.

## MODEL DEVELOPMENT

**Background Subtraction.** The absorbance at a certain wavelength, $A(\lambda)$, is given by

$$A(\lambda) = A_{\mathrm{bkg}}(\lambda) + \sum_{(n,m)} A_{(n,m)}(\lambda) \tag{1}$$

$A_{\mathrm{bkg}}(\lambda)$ is the background due to colloidal graphite and $\pi$-plasmon absorption.[28−30] $\sum_{(n,m)} A_{(n,m)}(\lambda)$ is the total absorbance of all the nanotubes at wavelength $\lambda$.

The following functional form is assumed for the background, with $b$ and $k$ as empirical fit parameters.[31]

$$A_{\mathrm{bkg}}(\lambda) = k/\lambda^{b} \tag{2}$$

The absorbance after background subtraction is

$$A_{\mathrm{sub}}(\lambda) = A(\lambda) - A_{\mathrm{bkg}}(\lambda) \tag{3}$$

The spectrum obtained after complete functionalization of the nanotubes, leaving no resolved absorption peaks, is expected to be solely due to the background. Figure 1 shows the regressed background matches the recovered baseline after functionalization, thus giving confidence in the functional form used.

**Spectral Fitting of Optical Transitions.** The Franck−Condon principle states that each electronic state has associated vibronic states.[32−34] Environmental[19,35−38] and excitonic effects[39−41] on the nanotube create intermediate electronic states. The major elec-

(22) Hertel, T.; Fasel, R.; Moos, G. *Appl. Phys. A* **2002**, *75*, 449−465.
(23) Hagen, A.; Hertel, T. *Nano Lett.* **2003**, *3*, 383−388.
(24) Hagen, A.; Moos, G.; Talalaev, V.; Hertel, T. *Appl. Phys. A* **2004**, *78*, 1137−1145.
(25) Zheng, M.; Jagota, A.; Strano, M. S.; Santos, A. P.; Barone, P.; Chou, S. G.; Diner, B. A.; Dresselhaus, M. S.; McLean, R. S.; Onoa, G. B.; Samsonidze, G. G.; Semke, E. D.; Usrey, M.; Walls, D. J. *Science* **2003**, *302*, 1545−1548.
(26) Strano, M. S.; Zheng, M.; Jagota, A.; Onoa, G. B.; Heller, D. A.; Barone, P. W.; Usrey, M. L. *Nano Lett.* **2004**, *4*, 543−550.
(27) Zheng, M.; Jagota, A.; Semke, E. D.; Diner, B. A.; McLean, R. S.; Lustig, S. R.; Richardson, R. E.; Tassi, N. G. *Nat. Mater.* **2003**, *2*, 338−342.
(28) Landi, B. J.; Ruf, H. J.; Evans, C. M.; Cress, C. D.; Raffaelle, R. P. *J. Phys. Chem. B* **2005**, *109*, 9952−9965.
(29) Lin, M. F.; Shung, K. W. K. *Phys. Rev. B* **1994**, *50*, 17744−17747.
(30) Lin, M. F. *Phys. Rev. B* **2000**, *62*, 13153−13159.
(31) Ryabenko, A. G.; Dorofeeva, T. V.; Zvereva, G. I. *Carbon* **2004**, *42*, 1523−1535.
(32) Gold, H. S.; Rechsteiner, C. E.; Buck, R. P. *Anal. Chem.* **1976**, *48*, 1540−1546.
(33) Bauman, R. P. *Absorption Spectroscopy*; John Wiley and Sons: New York, 1962.
(34) Eisberg, R.; Resnick, R. *Quantum Physics of Atoms, Molecule, Solids, Nucliei, and Particles*; John Wiley and Sons: New York, 1974.
(35) Barone, P.; Baik, S.; Heller, D. A.; Strano, M. S. *Nat. Mater.* **2005**, *4*, 86−92.
(36) Heller, D. A.; Baik, S.; Eurell, T. E.; Strano, M. S. *Adv. Mater.* **2005**, *17*, 2793−2799.
(37) Heller, D. A.; Jeng, E. S.; Yeung, T. K.; Martinez, B. M.; Moll, A. E.; Gastala, J. B.; Strano, M. S. *Science* **2006**, *311*, 508−511.
(38) Jeng, E. S.; Moll, A. E.; Roy, A. C.; Gastala, J. B.; Strano, M. S. *Nano Lett.* **2006**, *6*, 371−375.
(39) Wang, F.; Dukovic, G.; Brus, L. E.; Heinz, T. F. *Science* **2005**, *308*, 838−841.

tronic transition is accompanied by minor ones, thereby broadening the absorption line shape.

We compared the fits for nine absorption spectra with Gaussian, Lorentzian, and Voigt profiles.[42] It was observed that the latter two gave much lower errors than the Gaussian fits.[42] The Voigt line shape was chosen over the Lorentzian since it represents a combination of natural line broadening due to uncertainty in particle lifetimes and Doppler broadening due to a distribution of particle velocities.[34] The spectral contributions of the nanotubes from 490 to 1600 nm (2.53−0.775 eV) are therefore represented as Voigt line shapes in energy space with peak areas $C_N = \{C^{ii}_{(n,m)}\}$, peak centers $\{E^{(n,m)}_{ii}\}$, and full widths at half-maximums (fwhm) $\{\Gamma_{V,ii}\}$, where $ii$ represents the transition, i.e., $E^M_{11}$, $E^S_{22}$, or $E^S_{11}$. The transition energies are known from the spectral assignment.[10,13,15] Three regions are identified for HiPco SWNT: 400−600 nm for $E^M_{11}$ and 550−900 and 800−1600 nm for $E^S_{22}$ and $E^S_{11}$, respectively.[9] Unique values of $\Gamma_{V,ii}$ are assumed for the three regimes. The line shape for a nanotube as a function of energy is

$$P^{ii}_{(n,m)}(E) = \int_{-\infty}^{\infty} G^{ii}_{(n,m)}(E')L^{ii}_{(n,m)}(E - E')\,\mathrm{d}E' \quad (4a)$$

The Voigt profile is a convolution of Gaussian ($G^{ii}_{(n,m)}(E)$) and Lorentzian ($L^{ii}_{(n,m)}(E)$) line shapes, which represent Doppler and natural broadening of the spectral line, respectively. $G^{ii}_{(n,m)}(E)$ is centered at zero, while $L^{ii}_{(n,m)}(E)$ is centered at $E^{(n,m)}_{ii}$.

$$G^{ii}_{(n,m)}(E) = \frac{1}{\sqrt{2\pi}\sigma_{ii}}\exp\left[-\left(\frac{E}{\sqrt{2}\sigma_{ii}}\right)^2\right] \quad (4b)$$

$$\Gamma_{G,ii} = 2\sqrt{2\ln 2}\sigma_{ii} \quad (4c)$$

$$L^{ii}_{(n,m)}(E) = \frac{\Gamma_{L,ii}/2\pi}{(E - E^{(n,m)}_{ii})^2 + \Gamma^2_{L,ii}/4} \quad (4d)$$

where $\Gamma_{G,ii}$ and $\Gamma_{L,ii}$ are the fwhms of the Gaussian and Lorentzian, respectively, and $\sigma_{ii}$ is the standard deviation for the Gaussian. A relation between $\Gamma_{V,ii}$, $\Gamma_{G,ii}$, and $\Gamma_{L,ii}$ is given by[43]

$$\Gamma_{V,ii} = 0.5346\Gamma_{L,ii} + \sqrt{0.2166\Gamma^2_{L,ii} + \Gamma^2_{G,ii}} \quad (5a)$$

Assuming $\Gamma_{G,ii} \approx \Gamma_{L,ii}$ to reduce the number of fit parameters, we get

$$\Gamma_{G,ii} \approx \Gamma_{L,ii} \approx \frac{\Gamma_{V,ii}}{1.6376} \quad (5b)$$

For the $E^S_{11}$, $E^S_{22}$, and $E^M_{11}$ line shapes, the pairs ($E^{(n,m)}_{11}$,$\Gamma_{V,11}$), ($E^{(n,m)}_{22}$,$\Gamma_{V,22}$), and ($E^{(n,m)}_{M}$,$\Gamma_{V,M}$), respectively, are substituted in eqs 4a−d and 5a,b. $P^{ii}_{(n,m)}(E)$ can be expressed as a function of the wavelength, $\lambda$, by using the relation $E = hc/\lambda$, where $h$ is Planck's constant and $c$ is the velocity of light. After background subtraction, the overall absorbance at $\lambda$ is

$$A_{sub}(\lambda) = \sum_{(n,m)} C^{11}_{(n,m)}P^{11}_{(n,m)}(\lambda) + C^{22}_{(n,m)}P^{22}_{(n,m)}(\lambda) + C^{M}_{(n,m)}P^{M}_{(n,m)}(\lambda) \quad (6)$$

**Assumptions.** The deconvolution procedure is predicated on two major assumptions. A more detailed knowledge of each of the following aspects will enable the code to be more robust and rigorous.

**Fwhm.** The fwhms ($\Gamma_{V,11}$, $\Gamma_{V,22}$, $\Gamma_{V,M}$) are held constant for all nanotubes in a particular spectral region, although variation of the line widths with diameter, band structure, or energy is more likely. Due to the lack of information at present on the actual dependence of the fwhms on any of the above parameters, we have assumed constant peak widths. This dependence can easily be added to the code when known theoretically or experimentally.

**Weighting Scheme.** Each absorption peak is assumed to correspond to an individual Voigt function, which envelopes a certain number of nanotube transition energies. The set of these peak areas, $C_G$, contains the fitting parameters. The peak areas of the enveloped nanotubes are approximated as fractions of the peak area of the parent Voigt profile. Given a peak energy, $p_k(E)$, it is assumed that only the nanotubes with transition energies within the flanking valleys, $v_k(E)$ and $v_{k+1}(E)$, contribute to the peak in question. These contributions are assumed to depend on the proximity of their respective transition energies to $p_k(E)$, with the weighting factor of the $j$th nanotube under the $k$th parent Voigt profile being

$$\gamma_{jk} = \exp\left(-\frac{|E^j_{ii} - p_k(E)|}{v_{k+1}(E) - v_k(E)}\right) \quad (7)$$

These weights are normalized so that the parent Voigt line shape is a sum of the individual nanotube Voigt line shapes:

$$\omega_{jk} = \frac{\gamma_{jk}}{\sum_j \gamma_{jk}} \quad (8)$$

Approximate values for the spectral contribution of each ($n,m$) species, $C_N$, from $C_G$ are computed with the following transformation:

$$C_N = \Omega C_G \quad (9)$$

with the matrix $\Omega$ containing the normalized weights $\omega_{jk}$. Implicit in the weighting scheme is the assumption that the sample population is continuous and nonzero over the spectral range.

In each group of nanotubes with similar transition energies, the weighting scheme approximates the effect of the absorption coefficient, which determines the ($n,m$) dependence of the probability of absorption of radiation at different energies; how-


(40) Maultzsch, J.; Pomeraenke, R.; Reich, S.; Chang, E.; Prezzi, D.; Ruini, A.; Molinari, E.; Strano, M. S.; Thomsen, C.; Lienau, C. *Phys. Rev. B* **2005**, *72*, 241402.
(41) Reich, S.; Thomsen, C.; Robertson, J. *Phys. Rev. Lett.* **2005**, *95*, 077402.
(42) See Supplement.
(43) Olivero, J.; Longbothum, R. L. *J. Quant. Spectrosc. Radiat. Transfer* **1977**, *17*, 233.

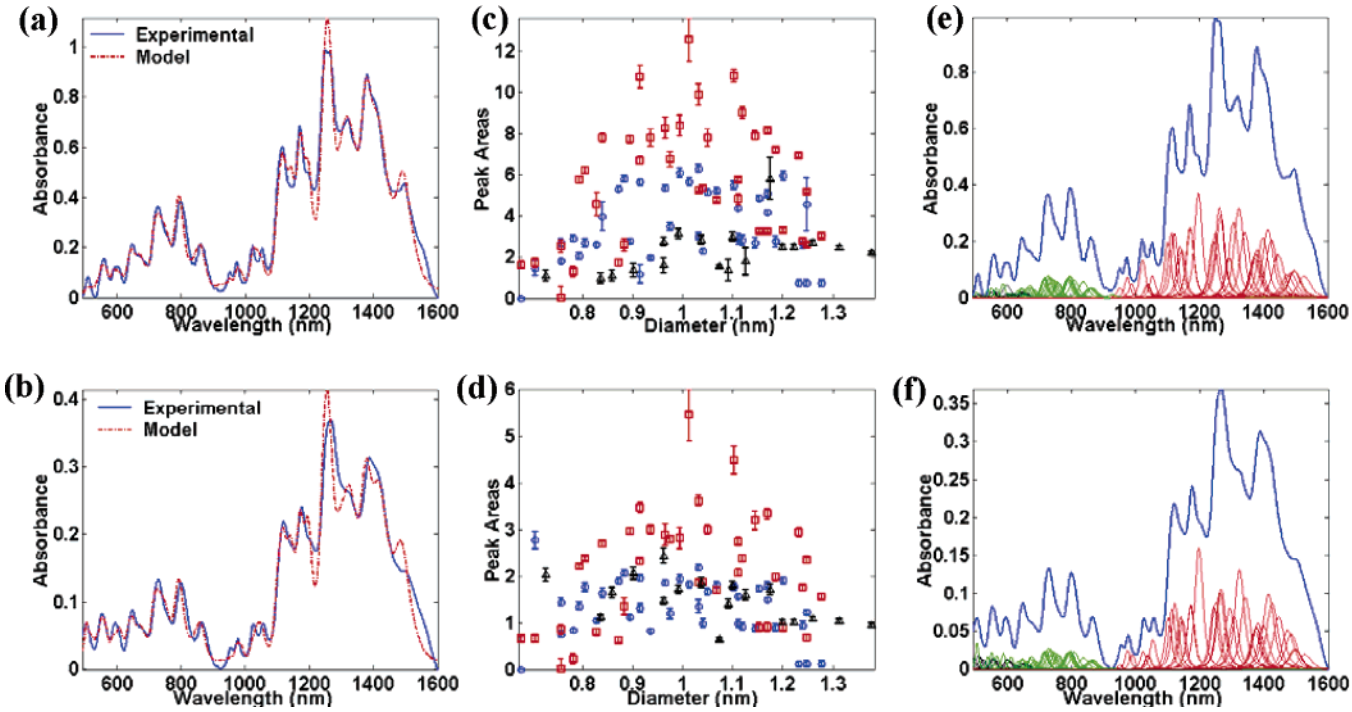


**Figure 2.** Fits of SDS-suspended HiPco nanotubes. (a) and (b) The solid blue line denotes the actual spectrum and the dotted red line represents the fit. (c) and (d) Confidence intervals corresponding to the 2 spectra, with the red squares denoting the $E_{11}$ peaks, blue circles denoting the $E_{22}$ peaks, and the black triangles denoting the metallic peaks. (e) and (f) The deconvoluted peaks for the spectra in (a) and (b), respectively.

ever, we have not included an explicit (*n,m*) variation of the absorption coefficient for the nanotubes considered.

**Confidence Intervals.** The 95% confidence intervals for the parameter estimates were computed with the Statistics Toolbox in MATLAB in conjunction with a code that used maximum likelihood estimation.[44−46] We fit ∼20 parameters—corresponding to 20 peaks—in a typical SDS-SWNT absorption spectrum. Tightly bound confidence intervals guarantee the uniqueness of the fit, although some compromise has to be made with regard to the quality of the fit. We note that it is possible to obtain a perfect fit by floating the peak areas, peak centers, and line widths; however, such a fit will not be unique and the corresponding confidence intervals will be large, implying large uncertainties in the parameter estimates. This work is the first to address spectral uniqueness for SWNT deconvolution.

The peak areas are proportional to the oscillator strengths of the individual nanotubes in the sample.[32] We have considered 57 nanotubes (39 semiconductors and 18 metals). Spectral deconvolution in this case is difficult because information content on specific nanotubes is distributed nonuniformly. The $E_{11}^{S}$ region is more informative than the $E_{22}^{S}$ or the $E_{11}^{M}$ because it covers a larger energy range and contains more well-defined peaks.

## RESULTS AND DISCUSSION

The deconvolution method was tested on the absorption spectra of the following: (1) unfunctionalized, selectively functionalized, and completely functionalized SDS-suspended HiPco SWNTs; (2) fractionated samples of DNA-SWNT; (3) CoMoCAT SWNT.[47] After obtaining reasonable fits and tight confidence intervals, the algorithm was used to analyze absorption spectra of electronically selective reactions of SWNT with diazonium reagents.[19,48]

**SDS-SWNT.** Approximate values for $\Gamma_{V,11}$ (29.86 meV), $\Gamma_{V,22}$ (57.96 meV), and $\Gamma_{V,M}$ (93.42 meV) were obtained from fits of the absorption spectra of DNA-HiPco SWNT separated by diameter using ion-exchange chromatography.[25−27,42] The weighting scheme relies heavily on the experimentally determined transition wavelengths as obtained for the SDS-SWNT system.[10,13−15] In the case of DNA-SWNT absorption spectra, the transition wavelength of each nanotube is red-shifted to a different extent,[26] thus adversely affecting the weighting scheme. The DNA-SWNT spectra we used had fewer nanotubes and were less complex than the SDS-SWNT spectra. Consequently, we were able to fit each nanotube peak individually, without weighting them.

A value of 25 meV for $\Gamma_{V,11}$ provided better agreement for SDS-SWNT spectra. This could be due to surfactant effects, which might affect the $E_{11}^{S}$ more than the $E_{22}^{S}$ or the $E_{11}^{M}$ due to greater electron screening in the latter two cases.[49] It also agrees with data reported in the literature.[9,24,50] A CoMoCAT SWNT spectral fit required a much higher value of $\Gamma_{V,11}$ (60 meV) for a reasonable

(44) Gunawan, R.; Jung, M. Y. L.; Seebauer, E. G.; Braatz, R. D. *AIChE J.* **2003**, *49*, 2114−2123.
(45) Beck, J. V.; Arnold, K. J. *Parameter Estimation in Engineering and Science*; John Wiley and Sons: New York, 1977.
(46) Nagy, Z. K.; Braatz, R. D. *IEEE Trans. Control Syst. Technol.* **2003**, *11*, 694−704.
(47) Kitiyanan, B.; Alvarez, W. E.; Harwell, J. H.; Resasco, D. E. *J. Catal.* **2001**, *204*, 129−145.
(48) Strano, M. S.; Dyke, C. A.; Usrey, M. L.; Barone, P. W.; Allen, M. J.; Shan, H.; Kittrell, C.; Hauge, R. H.; Tour, J. M.; Smalley, R. E. *Science* **2003**, *301*, 1519−1522.
(49) Huang, H.; Kajiura, H.; Maruyama, R.; Kadano, K.; Noda, K. *J. Phys. Chem. B* **2006**, *110*, 4686−4690.
(50) Hartschuh, A.; Pedrosa, H. N.; Novotny, L.; Krauss, T. D. *Science* **2003**, *301*, 1354−1356.

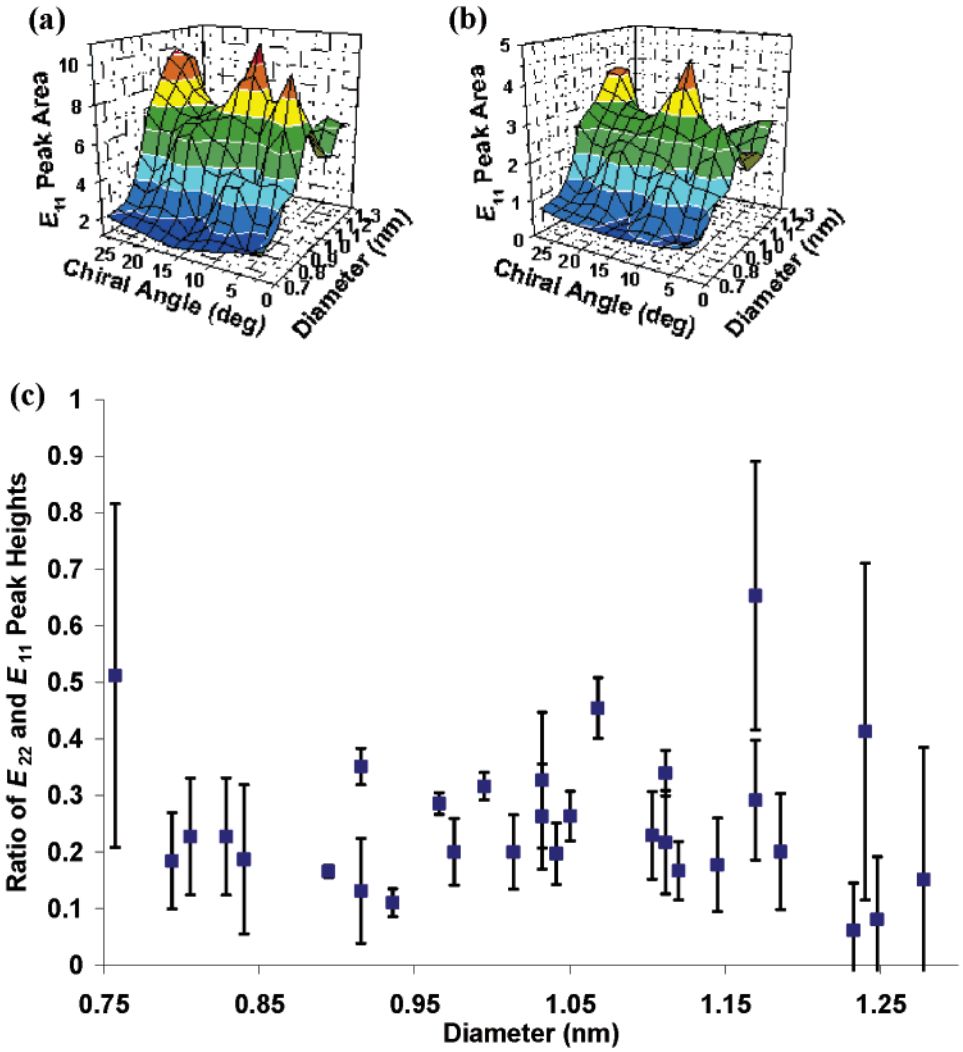


**Figure 3.** (a) 3-D plot of $E_{11}$ peak area vs diameter and chiral angle for the spectrum in Figure 2a. (b) $E_{11}$ peak area vs diameter and chiral angle for the spectrum in Figure 2b. The plots in (a) and (b) were compared with the fluorescence plots in Bachilo et al.[10] (c) Ratios of $E_{22}$ and $E_{11}$ peak heights for 30 semiconducting nanotubes were obtained from fits of 9 spectra.

fit.[42] This broadening could be due to the presence of inhomogeneous bundles of nanotubes.

Panels a and b in Figure 2 show the fits of the absorption data of two different SDS-HiPco SWNT samples. The associated diameter distributions of the calculated peak areas are shown in Figure 2c and d, respectively. The red squares denote the $E_{11}^{S}$ peak areas, the blue circles denote the $E_{22}^{S}$ peak areas, and the black triangles represent the $E_{11}^{M}$ peak areas. It should be noted that the parameter estimates are tightly bound, as observed by the small confidence intervals. Hence, despite the complexity of the spectrum, the obtained parameters are meaningful within the accuracy of the stated assumptions. Panels e and f in Figure 2 show the deconvoluted $E_{11}^{M}$, $E_{22}^{S}$, and $E_{11}^{S}$ peaks for the spectra in Figure 2a and b, respectively.

Panels a and b in Figure 3 show three-dimensional plots of the $E_{11}^{S}$ peak areas versus diameter and chiral angle for the deconvoluted spectra. The plots are qualitatively similar to the smoothed surface plot of fluorescence intensity as a function of nanotube diameter and chiral angle, as reported by Bachilo et al.;[10] however, panels a and b in Figure 3 do not show the reported trend with chiral angle, wherein the quantum yields are greater for near-armchair chiralities and nanotubes from the $(n - m)$-mod $3 = -1$ family.[10,41] This could be because photoabsorption is an ensemble measurement of nanotube concentrations, while photoluminescence is able to probe single nanotubes and, hence, extract chirality and diameter dependencies simultaneously. We note that the $(n,m)$ dependence of the quantum yield is not known and does not affect the absorption spectrum.

We expect the $E_{22}^{S}$ peak height of a particular nanotube to be lower than its corresponding $E_{11}^{S}$ peak height, simply because the $E_{11}^{S}$ transition is energetically more probable than the $E_{22}^{S}$ transition. To investigate this, we calculated the ratios of the $E_{22}^{S}$ and $E_{11}^{S}$ peak heights for nine SDS-HiPco SWNT spectra. Out of the 39 semiconductors considered, it was found that 30 of them had ratios that were less than unity. The results have been plotted, with error bars, versus diameter in Figure 3c. With the knowledge of such links between individual $E_{22}^{S}$ and $E_{11}^{S}$ peaks, future modifications to the algorithm could involve the generation of the $E_{22}^{S}$ portion of the absorption spectrum entirely from the $E_{11}^{S}$ region, thus reducing the number of fit parameters. Specifically, knowledge of these individual ratios would permit the relaxation of the diameter continuity constraint.

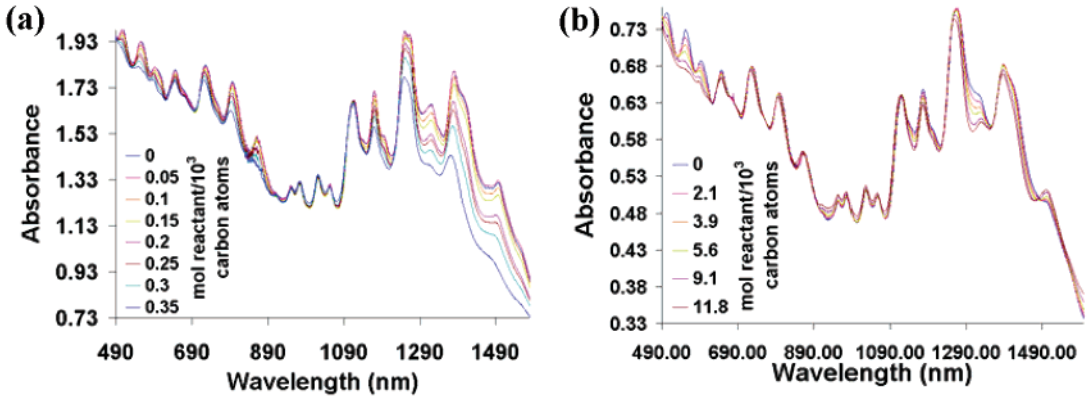


**Figure 4.** Two different sets of reaction spectra that were analyzed with the algorithm. (a) SWNT reaction carried out in a flow-through setup with 4-hydroxybenzene diazonium salt, as described in the Experimental Section. (b) SWNT reaction setup with 4-chlorobenzene diazonium salt, as described in Strano et al.[48]

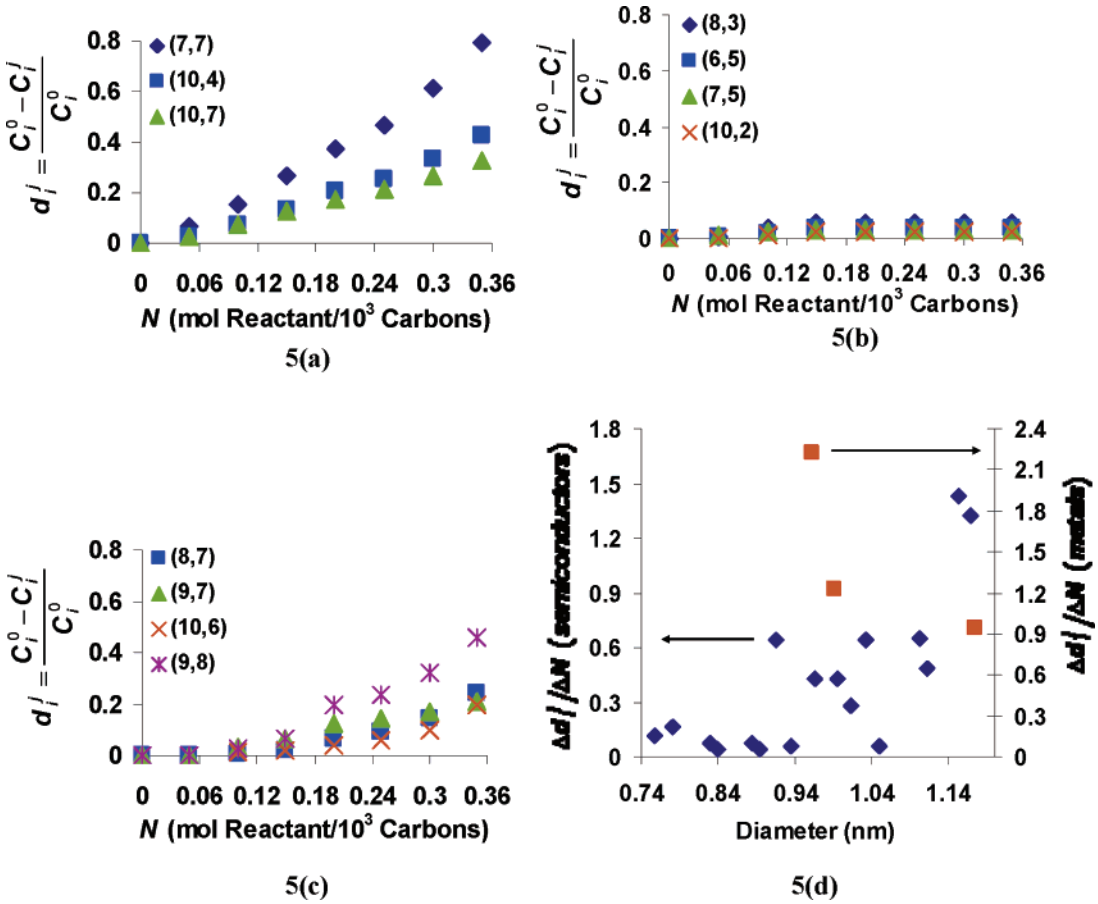


**Figure 5.** Analysis of reaction data shown in Figure 4a, where $d_i^j$ is the degree of functionalization. It represents the decrease in peak area of the *i*th nanotube, normalized to its starting peak area, after the *j*th addition of diazonium salt. *N* denotes the concentration diazonium reagent in the solution. The figures depict the effect of diazonium reaction on (a) metallic SWNTs; (b) small-diameter semiconducting SWNTs; (c) large-diameter semiconducting SWNTs; (d) slopes ($\Delta d_i^j/\Delta N$), as measures of reactivity, were calculated from the reaction data for 17 semiconducting nanotubes (blue diamonds) and 3 metallic nanotubes (orange squares) and plotted against diameter. A distinct trend is observed for the semiconductors, where reactivity increases with diameter.

**SWNT-Diazonium Reactions.** Figure 4a shows the steady-state photoabsorption spectra for the reaction setup described in the Experimental Section. Figure 4b shows data from Strano et al., where the reagent used was 4-chlorobenzene diazonium salt.[48] The algorithm was used to analyze both data sets as a demonstration of its utility.

Under selective reaction conditions, metallic tubes react with the diazonium compound first, followed by large-diameter semiconducting tubes, and finally by small-diameter semiconducting tubes.[48,51] This progression is clearly seen in the absorption spectra in Figure 4a and b. Nanotubes with similar band gaps will show similar trends in reactivity. According to our algorithm, the spectral contributions of nanotubes that are grouped under a certain absorption peak will decay at the same rate, since they

(51) Strano, M. S. *J. Am. Chem. Soc.* **2003**, *125*, 16148−16153.

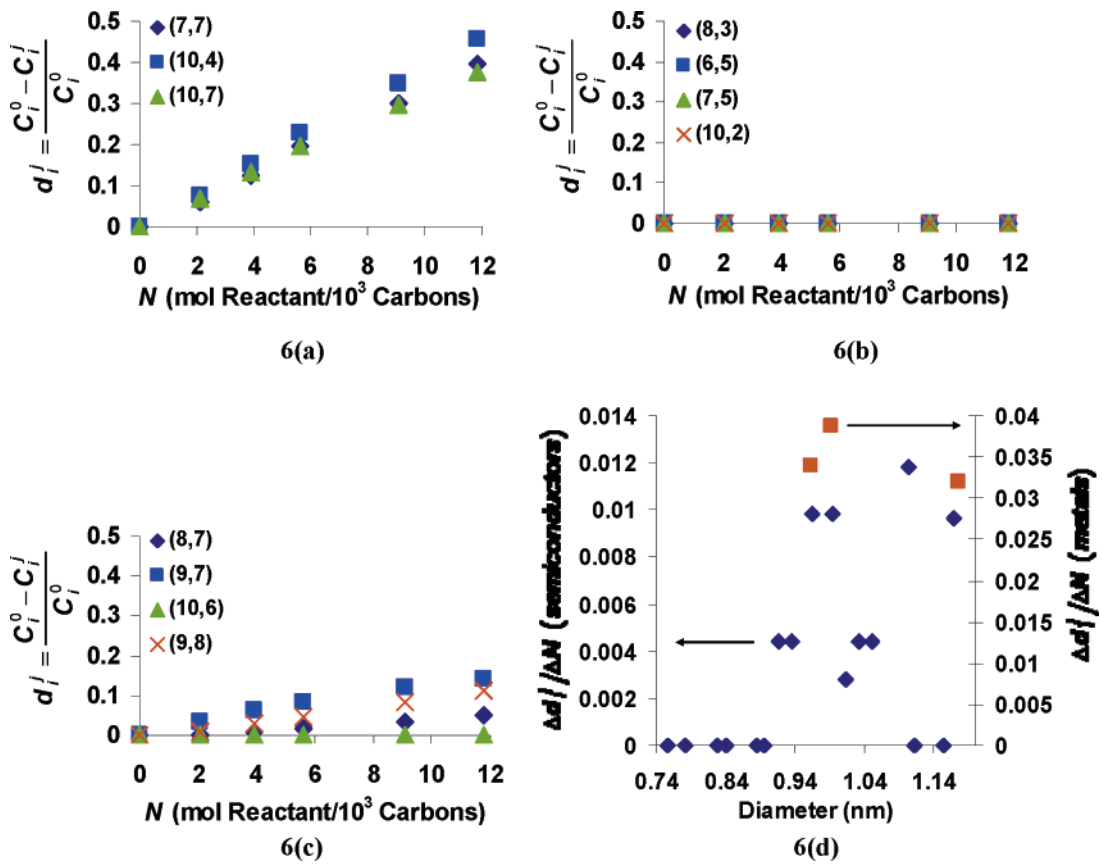


**Figure 6.** Analysis of reaction data shown in Figure 4b, where $d_i^j$ is the degree of functionalization. It represents the decrease in peak area of the *i*th nanotube, normalized to its starting peak area, after the *j*th addition of diazonium salt. *N* denotes the concentration diazonium reagent in the solution. The figures depict the effect of diazonium reaction on (a) metallic SWNTs; (b) small-diameter semiconducting SWNTs; (c) large-diameter semiconducting SWNTs; (d) slopes ($\Delta d_i^j/\Delta N$), as measures of reactivity, were calculated from the reaction data for 17 semiconducting nanotubes (blue diamonds) and 3 metallic nanotubes (orange squares) and plotted against diameter. A distinct trend is observed for the semiconductors, where reactivity increases with diameter.

are simply fractions of the total peak area, as derived in eq 9. It is difficult to obtain reactivity information on all the metallic nanotubes, since absorption features at wavelengths above 630 nm have considerable contributions from the $E_{22}^S$ peaks of semiconducting nanotubes. The low-energy ($E_{11}^S$) region is easier to analyze, since it is composed purely of $E_{11}^S$ peaks. Hence, as far as estimating rate constants for nanotube reactions is concerned, it is expected that more information will be available for semiconducting nanotubes.

We have measured the peak areas of three metallic tubes and four small-diameter and four large-diameter semiconductors with increasing diazonium addition for both the data sets considered. Figures 5 and 6 show the results of the analysis. The degree of functionalization, $d_i^j$, for the *i*th nanotube after the *j*th addition is

$$d_i^j = \frac{C_i^0 - C_i^j}{C_i^0} \tag{10}$$

$C_i^0$ and $C_i^j$ are the peak areas at the zeroth and *j*th addition steps, respectively. It can be seen that the degree of functionalization for metallic nanotubes increases linearly with diazonium addition (Figures 5a and 6a), while the small-diameter semiconductors remain almost unaffected (Figures 5b and 6b). The large-diameter semiconductors (Figures 5c and 6c) are more reactive than the small-diameter semiconductors but not to the same extent as the metals. In past work, we have shown that the reaction follows a two-step mechanism.[19] The first step (rate constant, $k_1$) is a selective, noncovalent adsorption of the diazonium on the SWNT. It depends on the density of states (DOS) at the Fermi level.[48] The second step is presumably a nonselective reaction in which a covalent bond is formed. A higher DOS gives a larger value of $k_1$, which yields a stronger linear relationship between $d_i^j$ and diazonium concentration. This explains the greater slopes for the plots of the metallic and large-diameter semiconducting tubes as compared to the small-diameter semiconductors. Slopes for the $d_i^j$ versus diazonium concentration data—$\Delta d_i^j/\Delta N$, where *N* is the concentration of diazonium salt in solution—were calculated for 17 semiconducting nanotubes and 3 metallic nanotubes, and the results are shown in Figures 5d and 6d. The blue diamonds represent semiconducting nanotubes and the orange squares denote metallic nanotubes, and they have been referred to different axes for clarity. Since more data are available for the semiconductors, we can see a definite trend wherein the slopes increase (i.e., reactivities increase) with increasing diameters. We note that our algorithm can be used to extract structure−reactivity relationships for a range of (*n*,*m*) nanotubes for various chemistries—an important step in understanding chemical reactivity in carbon nanotube systems. Subsequent work will attempt to establish a

more concrete link between the band structure of individual nanotubes and their respective degrees of functionalization.

## CONCLUSIONS

A generic algorithm has been presented and used to fit SDS-suspended HiPco SWNT, CoMoCat SWNT, and DNA-suspended HiPco SWNT fractionated by ion-exchange chromatography. The method has also been used to describe the selective decay of representative (*n,m*) peak areas upon reaction of HiPco SWNT with 4-chlorobenzene diazonium and 4-hydroxybenzene diazonium salts. The algorithm is able to spot trends in reactivity, especially for semiconducting nanotubes, since more information is available about distinct nanotubes in the $E_{11}^{S}$ region of the absorption spectrum as compared to the $E_{11}^{M}$ region. We realize that the proposed deconvolution procedure is a starting attempt at trying to understand the absorption spectrum of monodispersed nanotubes and obtain quantitative information related to nanotube reactions. Suitable amendments can be made to it as new discoveries concerning the photophysics of carbon nanotubes are made.

## ACKNOWLEDGMENT

M.S.S. acknowledges a CAREER Award from the National Science Foundation (grant CTS-0449147) and funding from Intel (class A). M.S.S. is also grateful for a 2004 DuPont Young Investigator Award. The authors thank R. B. Weisman, R. B. Hauge, C. Kittrell, A. Jorio, M. Dresselhaus, P. W. Barone, and D. A. Heller for useful discussions regarding this work. We have made the code and the required information on nanotube transition energies accessible to the general public via the Supporting Information.

## SUPPORTING INFORMATION AVAILABLE

Fits of DNA-SWNT and CoMoCat SWNT spectra, error comparison for fits using Gaussian, Lorentzian, and Voigt line shapes, the codes for fitting individual SWNT absorption spectra as well as those of SWNT-diazonium reactions, and instructions to use these codes. This material is available free of charge via the Internet at http://pubs.acs.org.

Received for review June 15, 2006. Accepted July 29, 2006.

AC0610917